

## Article

# Stabilization of Superionic-Conducting High-Temperature Phase of $\text{Li}(\text{CB}_9\text{H}_{10})$ via Solid Solution Formation with $\text{Li}_2(\text{B}_{12}\text{H}_{12})$

Sangryun Kim <sup>1,\*</sup>, Kazuaki Kisu <sup>2</sup> and Shin-ichi Orimo <sup>1,2,\*</sup><sup>1</sup> Institute for Materials Research, Tohoku University, Sendai 980-8577, Japan<sup>2</sup> WPI-Advanced Institute for Materials Research (WPI-AIMR), Tohoku University, Sendai 980-8577, Japan; k.kisu@imr.tohoku.ac.jp

\* Correspondence: sangryun@imr.tohoku.ac.jp (S.K.); orimo@imr.tohoku.ac.jp (S.-i.O.)

**Abstract:** We report the stabilization of the high-temperature (high- $T$ ) phase of lithium carba-*closo*-decaborate,  $\text{Li}(\text{CB}_9\text{H}_{10})$ , via the formation of solid solutions in a  $\text{Li}(\text{CB}_9\text{H}_{10})$ - $\text{Li}_2(\text{B}_{12}\text{H}_{12})$  quasi-binary system.  $\text{Li}(\text{CB}_9\text{H}_{10})$ -based solid solutions in which  $[\text{CB}_9\text{H}_{10}]^-$  is replaced by  $[\text{B}_{12}\text{H}_{12}]^{2-}$  were obtained at compositions with low  $x$  values in the  $(1-x)\text{Li}(\text{CB}_9\text{H}_{10})-x\text{Li}_2(\text{B}_{12}\text{H}_{12})$  system. An increase in the extent of  $[\text{B}_{12}\text{H}_{12}]^{2-}$  substitution promoted stabilization of the high- $T$  phase of  $\text{Li}(\text{CB}_9\text{H}_{10})$ , resulting in an increase in the lithium-ion conductivity. Superionic conductivities of over  $10^{-3} \text{ S cm}^{-1}$  were achieved for the compounds with  $0.2 \leq x \leq 0.4$ . In addition, a comparison of the  $\text{Li}(\text{CB}_9\text{H}_{10})$ - $\text{Li}_2(\text{B}_{12}\text{H}_{12})$  system and the  $\text{Li}(\text{CB}_9\text{H}_{10})$ - $\text{Li}(\text{CB}_{11}\text{H}_{12})$  system suggests that the valence of the complex anions plays an important role in the ionic conduction. In battery tests, an all-solid-state  $\text{Li}$ - $\text{TiS}_2$  cell employing  $0.6\text{Li}(\text{CB}_9\text{H}_{10})-0.4\text{Li}_2(\text{B}_{12}\text{H}_{12})$  ( $x = 0.4$ ) as a solid electrolyte presented reversible battery reactions during repeated discharge-charge cycles. The current study offers an insight into strategies to develop complex hydride solid electrolytes.

**Keywords:** complex hydride; solid electrolyte; all-solid-state battery; superionic conductor; phase transition; high-temperature phase



**Citation:** Kim, S.; Kisu, K.; Orimo, S.-i. Stabilization of Superionic-Conducting High-Temperature Phase of  $\text{Li}(\text{CB}_9\text{H}_{10})$  via Solid Solution Formation with  $\text{Li}_2(\text{B}_{12}\text{H}_{12})$ . *Crystals* **2021**, *11*, 330. <https://doi.org/10.3390/cryst11040330>

Academic Editors: Zhao Qian, Hai-Wen Li and Abdel El-kharbachi

Received: 19 February 2021

Accepted: 24 March 2021

Published: 25 March 2021

**Publisher's Note:** MDPI stays neutral with regard to jurisdictional claims in published maps and institutional affiliations.



**Copyright:** © 2021 by the authors. Licensee MDPI, Basel, Switzerland. This article is an open access article distributed under the terms and conditions of the Creative Commons Attribution (CC BY) license (<https://creativecommons.org/licenses/by/4.0/>).

## 1. Introduction

All-solid-state batteries, in which both the electrolyte and electrodes are solids, are promising candidates for resolving the intrinsic drawbacks of conventional liquid electrolyte-based batteries, such as flammability, limited voltage window, and low energy density [1–6]. Solid electrolytes are one of the key materials of all-solid-state batteries because their ionic conductivity and chemical/electrochemical stability greatly affect the battery performance [7–10]. Among the variety of materials reported to date, complex hydrides, generally denoted by  $M_x(M'_y\text{H}_z)$  (where  $M$  is a metal cation and  $M'_y\text{H}_z$  is a complex anion), have recently received discernible attention as a new solid electrolyte system, owing to their high ionic conductivity, high deformability, and superior chemical/electrochemical stability [3,11–15]. In addition, complex hydrides exhibit remarkably low material densities compared with other solid electrolyte systems, which is beneficial for fabricating high-energy density batteries.

A common characteristic (observed in most existing materials) of complex hydrides is a significant rise in the ionic conductivity by the phase transition accompanied by their structural change from an ordered low-temperature (low- $T$ ) phase to a disordered high- $T$  phase. On the basis of this phenomenon, initial studies of complex hydrides focused on lithium borohydride ( $\text{Li}(\text{BH}_4)$ ) and its derivatives.  $\text{Li}(\text{BH}_4)$  undergoes a phase transition to the high- $T$  phase at  $\approx 390 \text{ K}$ , accompanied by a substantial increase in conductivity; the high- $T$  phase of  $\text{Li}(\text{BH}_4)$  exhibits an ionic conductivity of over  $10^{-3} \text{ S cm}^{-1}$ , which is three orders of magnitude higher than that of its low- $T$  phase [11]. In addition, various

approaches have been explored for improving the ionic conductivity of Li(BH<sub>4</sub>)-based compounds; effective approaches reported thus far include substituting halide ions such as Cl<sup>−</sup>, Br<sup>−</sup>, and I<sup>−</sup> [16]; nanosizing [17]; using thin films [18]; preparing solid solutions with Li(NH<sub>2</sub>) [19]; and using neutral ligands [20].

To further improve the ionic conductivities of complex hydrides, researchers have recently investigated a series of *closo*-type (cage-like) complex hydrides such as Li(CB<sub>9</sub>H<sub>10</sub>), Li(CB<sub>11</sub>H<sub>12</sub>), and Li<sub>2</sub>(B<sub>12</sub>H<sub>12</sub>) [21–24]. Compared to Li(BH<sub>4</sub>)-based complex hydrides, *closo*-type hydrides present an intrinsic advantage in ionic conduction because of the large and polyanionic structure of complex anions, which provides conduction channels for facile ionic diffusion with a low activation energy. Indeed, the ionic conductivities of high-*T* phases of *closo*-type complex hydrides exceed 10<sup>−1</sup> S cm<sup>−1</sup>, which is two orders of magnitude higher than those of Li(BH<sub>4</sub>)-based compounds.

Among the numerous *closo*-type complex hydrides studied thus far, the high-*T* phase (space group *P31c*) of Li(CB<sub>9</sub>H<sub>10</sub>) has been studied most extensively as a solid electrolyte because of its low phase-transition temperature (90 °C) and high lithium-ion conductivity (8.1 × 10<sup>−2</sup> S cm<sup>−1</sup> at 110 °C) [22]. In particular, a recent study clarified that partial substitutions of the [CB<sub>9</sub>H<sub>10</sub>]<sup>−</sup> complex anions in Li(CB<sub>9</sub>H<sub>10</sub>) with [CB<sub>11</sub>H<sub>12</sub>]<sup>−</sup> complex anions (i.e., the low-*y* region in the (1-*y*)Li(CB<sub>9</sub>H<sub>10</sub>)-*y*Li(CB<sub>11</sub>H<sub>12</sub>) system) enable a disordered structure (hexagonal framework) the same as that of the high-*T* phase of Li(CB<sub>9</sub>H<sub>10</sub>) to be stabilized at room temperature [3,25]. Importantly, the stabilized high-*T* phases exhibit lithium superionic conductivities of over 10<sup>−3</sup> S cm<sup>−1</sup> at 25 °C. Furthermore, 0.7Li(CB<sub>9</sub>H<sub>10</sub>)-0.3Li(CB<sub>11</sub>H<sub>12</sub>) (*y* = 0.3) exhibits excellent chemical/electrochemical stability against high energy density lithium metal anode (theoretical capacity = 3860 mAh g<sup>−1</sup>, potential = −3.04 V vs. standard hydrogen electrode) [3].

The unique properties of the *closo*-type complex hydrides with respect to ionic conduction and electrochemical stability can open a new research area in the field of solid electrolyte materials of all-solid-state batteries. In this regard, gaining a systematic understanding of the high-*T* phase for various *closo*-type complex hydride systems and how their compositions affect the resulting material properties is important for developing wide-ranging material varieties, which is an essential step toward realizing practical applications of all-solid-state batteries [26]. However, the high-*T* phase of Li(CB<sub>9</sub>H<sub>10</sub>) has only been investigated for the Li(CB<sub>9</sub>H<sub>10</sub>)-Li(CB<sub>11</sub>H<sub>12</sub>) system to date [3,25,27]. In addition, from the application point of view, reducing the carba-*closo*-boranes, which require the cost-expensive synthetic process, is one of the important challenges.

In the present work, we report stabilization of the high-*T* phase of Li(CB<sub>9</sub>H<sub>10</sub>) via solid solution formations of Li(CB<sub>9</sub>H<sub>10</sub>) and Li<sub>2</sub>(B<sub>12</sub>H<sub>12</sub>). Our investigations indicate that the Li(CB<sub>9</sub>H<sub>10</sub>)-based phases were formed in the low *x* region of the (1-*x*)Li(CB<sub>9</sub>H<sub>10</sub>)-*x*Li<sub>2</sub>(B<sub>12</sub>H<sub>12</sub>) quasi-binary system and that increasing *x* facilitated stabilization of the high-*T* phase. In addition, all-solid-state Li-TiS<sub>2</sub> batteries fabricated using 0.6Li(CB<sub>9</sub>H<sub>10</sub>)-0.4Li<sub>2</sub>(B<sub>12</sub>H<sub>12</sub>) (*x* = 0.4) as a solid electrolyte were demonstrated to exhibit good cycling stability.

## 2. Materials and Methods

### 2.1. Synthesis

The starting materials, Li(CB<sub>9</sub>H<sub>10</sub>) and Li<sub>2</sub>(B<sub>12</sub>H<sub>12</sub>), were obtained by drying Li(CB<sub>9</sub>H<sub>10</sub>)·*x*H<sub>2</sub>O (Katchem Ltd.) at 200 °C for 12 h and Li<sub>2</sub>(B<sub>12</sub>H<sub>12</sub>)·*x*H<sub>2</sub>O (Katchem Ltd.) at 225 °C for 20 h. Li(CB<sub>9</sub>H<sub>10</sub>) and Li<sub>2</sub>(B<sub>12</sub>H<sub>12</sub>) were first weighed in appropriate molar ratios and ground for 15 min using a mortar and pestle. The mixed powders were then ball-milled using a planetary ball mill (Pulverisette 7, Fritsch) at 400 rpm for 100 h. The low-speed condition of 400 rpm was used to prevent the decomposition during synthesis [28].

### 2.2. Characterization

Phase analysis was performed with X-ray diffraction (XRD, X'PERT Pro, PANalytical, Worcestershire, UK) measurements with CuKα radiation. Differential thermal analysis

(DTA) was performed using a Rigaku Thermo Plus TG-8120 system (TG-DTA 8120, Rigaku, Tokyo, Japan) from 25 to 150 °C at a ramp rate of 5 °C min<sup>-1</sup> under an Ar flow. Morphologies and particle sizes were analyzed using field-emission scanning electron microscopy (FE-SEM; SU9000, Hitachi, Tokyo, Japan).

The ionic conductivity was measured by the AC impedance method using a frequency response analyzer (3532-80, Hioki, Nagano, Japan) over a temperature range of 25–110 °C and a frequency range of 4 Hz to 1 MHz. The electrochemical stability was evaluated by cyclic voltammetry (CV; 1470E, Solartron Analytical, Wokingham, UK) using a Mo/0.6Li(CB<sub>9</sub>H<sub>10</sub>)–0.4Li<sub>2</sub>(B<sub>12</sub>H<sub>12</sub>)/Li cell in the scan range from –0.1 to 5 V (vs. Li<sup>+</sup>/Li). Li plating/stripping cycling was conducted with a Li/0.6Li(CB<sub>9</sub>H<sub>10</sub>)–0.4Li<sub>2</sub>(B<sub>12</sub>H<sub>12</sub>)/Li cell at a current density of 0.2 mA cm<sup>-2</sup> using a battery tester (580 Battery Test System, Scribner Associates, Southern Pines, NC, USA). Mo foil (Nilaco) and Li foil (Honjo Metal) were used as electrodes of the Mo/0.6Li(CB<sub>9</sub>H<sub>10</sub>)–0.4Li<sub>2</sub>(B<sub>12</sub>H<sub>12</sub>)/Li and Li/0.6Li(CB<sub>9</sub>H<sub>10</sub>)–0.4Li<sub>2</sub>(B<sub>12</sub>H<sub>12</sub>)/Li cells. For comparison, the same electrodes as in our previous studies [3,25] were used. Al and Cu foils were added to the cathode and anode sides, respectively, to avoid direct contacts between the cell and the pressing die.

For impedance cell fabrication, 70 mg of the 0.6Li(CB<sub>9</sub>H<sub>10</sub>)–0.4Li<sub>2</sub>(B<sub>12</sub>H<sub>12</sub>) powder was placed into a 10 mm diameter Teflon guide and uniaxially pressed at 38.4 MPa. The electrodes were transferred onto the pressed sample still present in the Teflon guide and uniaxially pressed again at 153.6 MPa to prepare pellet-type cells.

### 2.3. Battery Test

Battery tests were performed with a TiS<sub>2</sub>/0.6Li(CB<sub>9</sub>H<sub>10</sub>)–0.4Li<sub>2</sub>(B<sub>12</sub>H<sub>12</sub>)/Li cell. To avoid side reactions between electrodes and solid electrolytes [12,29], we used TiS<sub>2</sub> with a mild operating voltage (2.1 V vs. Li<sup>+</sup>/Li) as a cathode. For cathode composite fabrication, TiS<sub>2</sub> and 0.6Li(CB<sub>9</sub>H<sub>10</sub>)–0.4Li<sub>2</sub>(B<sub>12</sub>H<sub>12</sub>) were mixed in a 4:6 mass ratio (wt %) using an agate mortar and pestle for 15 min. For battery fabrication, 70 mg of the 0.6Li(CB<sub>9</sub>H<sub>10</sub>)–0.4Li<sub>2</sub>(B<sub>12</sub>H<sub>12</sub>) powder was placed into a 10 mm diameter Teflon guide and uniaxially pressed at 38.4 MPa. Subsequently, ≈10 mg of the cathode composite powder and lithium foil anode were then transferred onto opposite sides of the solid electrolyte and uniaxially pressed again at 153.6 MPa to prepare pellet-type cells. The cells were cycled in the voltage range of 1.6–2.7 V (vs. Li<sup>+</sup>/Li) at 60 °C using an electrochemical analyzer (580 Battery Test System, Scribner Associates, Southern Pines, NC, USA). The C-rate in this study is defined on the basis of 1 C = 239 mA g<sup>-1</sup>. For the calculation of the gravimetric capacities and currents, we only took into account the mass of the TiS<sub>2</sub> cathode.

## 3. Results and Discussion

### 3.1. Synthesis and Characterization

The complex hydrides in the quasi-binary system between Li(CB<sub>9</sub>H<sub>10</sub>) and Li<sub>2</sub>(B<sub>12</sub>H<sub>12</sub>) are described as (1–*x*)Li(CB<sub>9</sub>H<sub>10</sub>)–*x*Li<sub>2</sub>(B<sub>12</sub>H<sub>12</sub>). In this notation, the ratio (1–*x*):*x* indicates the molar ratio of [CB<sub>9</sub>H<sub>10</sub>]<sup>–</sup> and [B<sub>12</sub>H<sub>12</sub>]<sup>2–</sup> complex anions (Figure 1a). Compositions *x* = 0 and *x* = 1 represent the end-members, Li(CB<sub>9</sub>H<sub>10</sub>) and Li<sub>2</sub>(B<sub>12</sub>H<sub>12</sub>), respectively.

In general, material compositions play a critical role in the formation of solid solutions and the consequent structural changes [16,25,26]. Recent studies on the (1–*y*)Li(CB<sub>9</sub>H<sub>10</sub>)–*y*Li(CB<sub>11</sub>H<sub>12</sub>) system have indicated that the substitution of [CB<sub>11</sub>H<sub>12</sub>]<sup>–</sup> complex anions for the [CB<sub>9</sub>H<sub>10</sub>]<sup>–</sup> complex anions in Li(CB<sub>9</sub>H<sub>10</sub>) is achieved only at compositions with low *y* [25]. Inspired by these results, we focused mainly on the low-*x* region (0.1 ≤ *x* ≤ 0.5) of the (1–*x*)Li(CB<sub>9</sub>H<sub>10</sub>)–*x*Li<sub>2</sub>(B<sub>12</sub>H<sub>12</sub>) system in this study.

Figure 1b shows XRD patterns of (1–*x*)Li(CB<sub>9</sub>H<sub>10</sub>)–*x*Li<sub>2</sub>(B<sub>12</sub>H<sub>12</sub>) prepared in the range 0.1 ≤ *x* ≤ 0.5, together with those of Li(CB<sub>9</sub>H<sub>10</sub>) (*x* = 0) and Li<sub>2</sub>(B<sub>12</sub>H<sub>12</sub>) (*x* = 1). The two main peaks, which were observed at approximately 14.9 and 17.1° for the low-*T* phase of Li(CB<sub>9</sub>H<sub>10</sub>) (*x* = 0), shifted to lower angles as *x* increased in the range 0.1 ≤ *x* ≤ 0.4. The characteristic difference in the XRD profiles between the high-*T* phase and the low-*T* phase of Li(CB<sub>9</sub>H<sub>10</sub>) (*x* = 0) was a new peak observed at ≈16.4°, which was assigned to the 002

peak of the high- $T$  phase (space group  $P31c$ ) [3,27]. In the range  $0.1 \leq x \leq 0.4$ , as the  $x$  value increased, this peak shifted to lower angles and its intensity increased (arrow in Figure 1b). These results indicate that, with an increase in  $x$ , the extent of  $[\text{B}_{12}\text{H}_{12}]^{2-}$  substitution for  $[\text{CB}_9\text{H}_{10}]^-$  increased, promoting stabilization of the high- $T$  phase. The successive lattice expansion ( $V = 211.2 \text{ \AA}^3$  at  $x = 0.1$  and  $V = 234.7 \text{ \AA}^3$  at  $x = 0.4$ ) with increasing  $x$  (Figure S1) also confirmed the formation of solid-solution phases of starting materials. When  $x$  was further increased, the  $\text{Li}_2(\text{B}_{12}\text{H}_{12})$ -based phase (mainly, low- $T$  phase) was formed ( $x = 0.5$ ).

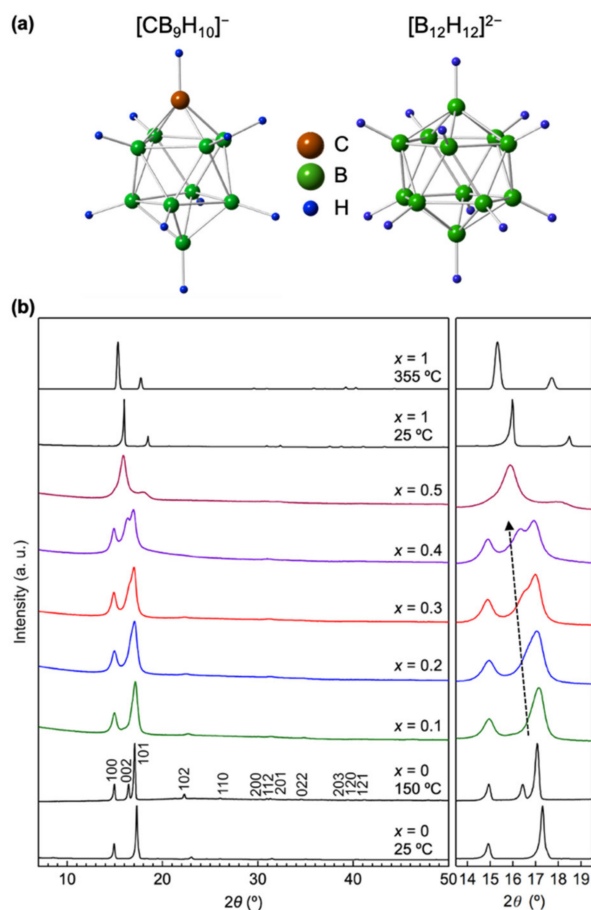


**Figure 1.** (a) Geometries of  $[\text{CB}_9\text{H}_{10}]^-$  and  $[\text{B}_{12}\text{H}_{12}]^{2-}$  complex anions. The brown, green, and blue spheres represent C, B, and H atoms, respectively. (b) XRD patterns for  $(1-x)\text{Li}(\text{CB}_9\text{H}_{10})-x\text{Li}_2(\text{B}_{12}\text{H}_{12})$  ( $0.1 \leq x \leq 0.5$ ) at room temperature, together with those of  $\text{Li}(\text{CB}_9\text{H}_{10})$  at room temperature and  $150 \text{ }^\circ\text{C}$ , and  $\text{Li}_2(\text{B}_{12}\text{H}_{12})$  at room temperature and  $355 \text{ }^\circ\text{C}$  (left). Enlarged XRD patterns in the low-angle region (right).

The phase transition between the low- $T$  and high- $T$  phases was investigated by DTA (Figure 2). The DTA profile for  $\text{Li}(\text{CB}_9\text{H}_{10})$  ( $x = 0$ ) cycled between  $25$  and  $150 \text{ }^\circ\text{C}$  exhibited endothermic and exothermic peaks at around  $60$  to  $90 \text{ }^\circ\text{C}$  upon heating–cooling cycling, which originated from phase transitions to and from the high- $T$  phase. Importantly, the  $0.1 \leq x \leq 0.4$  compounds displayed reduced DTA peak intensities. In addition, the peak intensities gradually decreased as  $x$  increased ( $0.1 \leq x \leq 0.4$ ) (the enlarged DTA curves are shown in Figure S2). These results reconfirm that, with increasing extent of complex anion substitutions, the high- $T$  phase formation is progressed. By contrast, the  $x = 0.5$  compound showed broader DTA peaks, which were ascribed to the phase transition of the  $\text{Li}_2(\text{B}_{12}\text{H}_{12})$ -based phase. In all of the compounds ( $0.1 \leq x \leq 0.5$ ), their precise phase-transition temperature could not be evaluated due to the broad peak profiles.

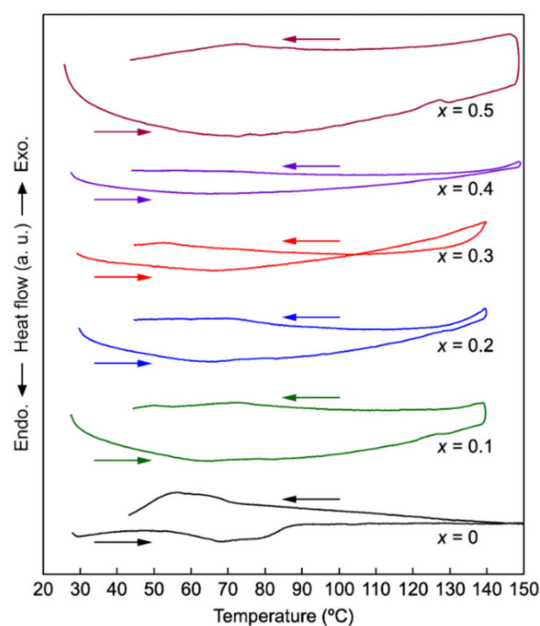


**Figure 2.** Differential thermal analysis (DTA) curves for  $(1-x)\text{Li}(\text{CB}_9\text{H}_{10})-x\text{Li}_2(\text{B}_{12}\text{H}_{12})$  ( $0 \leq x \leq 0.5$ ).

### 3.2. Ionic Conductivity

The ionic conductivities were assessed using electrochemical impedance spectroscopy (EIS) method. Figure 3 shows the lithium-ion conductivities of the  $(1-x)\text{Li}(\text{CB}_9\text{H}_{10})-x\text{Li}_2(\text{B}_{12}\text{H}_{12})$  compounds. Their room temperature conductivities and activation energies are summarized in Table S1.

The EIS measurements for the  $0.1 \leq x \leq 0.4$  compounds indicate that the room temperature ( $25\text{ }^\circ\text{C}$ ) conductivity increased with increasing  $x$ . In addition, Arrhenius plots of the ionic conductivities confirmed that, as  $x$  increased in the range  $0.1 \leq x \leq 0.4$ , the magnitude of the increase in conductivity originating from a phase transition was gradually diminished (Figure 3b and Figure S3). In particular, the Arrhenius plots for the compounds with  $x = 0.3$  and  $0.4$  almost displayed linear lines of the ionic conductivities. The room temperature conductivity and the activation energy of the  $x = 0.4$  compound were  $1.7 \times 10^{-3}\text{ S cm}^{-1}$  and  $40.3\text{ kJ mol}^{-1}$ , respectively (Table S1).

From the XRD patterns of the members of this composition region (Figure 1b), we found an increase in  $x$  led to an increase in the extent of complex anion substitution, which tended to gradually stabilize the high- $T$  phase. Therefore, we conclude that the increase in the conductivity for the compounds with  $0.1 \leq x \leq 0.4$  was the result of the high- $T$  phase stabilization according to the solid solution formations between  $\text{Li}(\text{CB}_9\text{H}_{10})$  ( $x = 0$ ) and  $\text{Li}_2(\text{B}_{12}\text{H}_{12})$  ( $x = 1$ ).

When  $x$  was increased beyond  $0.4$ , the change in conductivity tended to vary in the opposite direction from the change in conductivity in the region  $0.1 \leq x \leq 0.4$ . The  $x = 0.5$  compound exhibited a lower conductivity than the  $x = 0.4$  compound (Figure 3a and Table S1). Moreover, the increase in conductivity originating from the phase transition reappeared at  $x = 0.5$  (Figure 3b). This conductivity change between  $x = 0.4$  and  $0.5$  can be explained by the structural change of the  $\text{Li}_2(\text{B}_{12}\text{H}_{12})$ -based phase (Figure 1b). These also agree well with the reappeared phase transitions in the DTA measurements (Figure 2).

For the  $(1-y)\text{Li}(\text{CB}_9\text{H}_{10})-y\text{Li}(\text{CB}_{11}\text{H}_{12})$  system, the solid solution effects on the phase transition were most noticeable in the low- $y$  region [3,25]. Indeed, the  $0.7\text{Li}(\text{CB}_9\text{H}_{10})-0.3\text{Li}(\text{CB}_{11}\text{H}_{12})$  ( $y = 0.3$ ) solid solution had a structural framework identical to that of the high- $T$  phase of  $\text{Li}(\text{CB}_9\text{H}_{10})$  ( $x = 0$ ). In addition, the ionic conductivities of  $0.7\text{Li}(\text{CB}_9\text{H}_{10})-0.3\text{Li}(\text{CB}_{11}\text{H}_{12})$  ( $y = 0.3$ ) matched well with those of  $\text{Li}(\text{CB}_9\text{H}_{10})$  ( $x = 0$ ); their activation energies were  $28.4$  ( $0.7\text{Li}(\text{CB}_9\text{H}_{10})-0.3\text{Li}(\text{CB}_{11}\text{H}_{12})$  ( $y = 0.3$ )) and  $28.9$  ( $\text{Li}(\text{CB}_9\text{H}_{10})$  ( $x = 0$ ))  $\text{kJ mol}^{-1}$ , respectively. In the present investigation, we determined that the high- $T$  phase of  $\text{Li}(\text{CB}_9\text{H}_{10})$

( $x = 0$ ) for the  $(1-x)\text{Li}(\text{CB}_9\text{H}_{10})-x\text{Li}_2(\text{B}_{12}\text{H}_{12})$  series was also stabilized in the low- $x$  region. However,  $0.6\text{Li}(\text{CB}_9\text{H}_{10})-0.4\text{Li}_2(\text{B}_{12}\text{H}_{12})$  ( $x = 0.4$ ) exhibited a higher activation energy ( $40.3 \text{ kJ mol}^{-1}$ ) than the previous ones. Furthermore, its ionic conductivity at  $25^\circ\text{C}$  ( $1.7 \times 10^{-3} \text{ S cm}^{-1}$ ) was lower than that ( $6.7 \times 10^{-3} \text{ S cm}^{-1}$ ) of  $0.7\text{Li}(\text{CB}_9\text{H}_{10})-0.3\text{Li}(\text{CB}_{11}\text{H}_{12})$ . These conductivity changes could plausibly result from the differences in the valences of the constituent complex anions [30]. The high valence caused strong electrostatic interactions with the counter ions, leading to sluggish ionic diffusion. On this basis, the relatively inferior ionic conduction of  $0.6\text{Li}(\text{CB}_9\text{H}_{10})-0.4\text{Li}_2(\text{B}_{12}\text{H}_{12})$  ( $x = 0.4$ ) was ascribed mainly to the bivalency of the  $[\text{B}_{12}\text{H}_{12}]^{2-}$  complex anions. These results also highlight that simultaneously achieving the high- $T$  phase formation and high ionic conductivity of the formed high- $T$  phase is imperative for the development of complex hydride ionic conductors. In such a case, a detailed structural characterization that clarifies interactions between the complex anions and the cations (Li, Na, Mg, etc.) may be needed to control both the high- $T$  phase stability and the ionic conductivity.

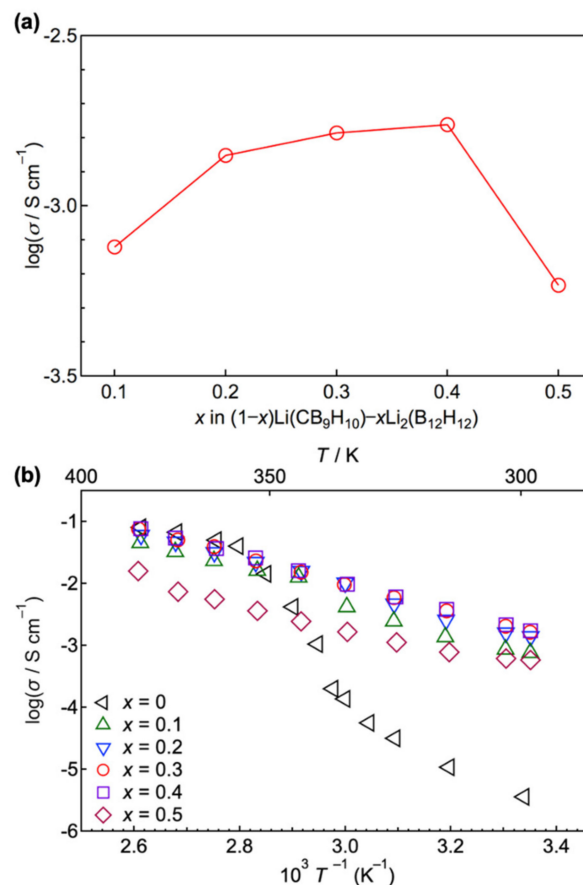


**Figure 3.** (a) Lithium-ion conductivities at  $25^\circ\text{C}$  and (b) arrhenius plots of the lithium-ion conductivities for  $(1-x)\text{Li}(\text{CB}_9\text{H}_{10})-x\text{Li}_2(\text{B}_{12}\text{H}_{12})$  ( $0.1 \leq x \leq 0.5$ ).

### 3.3. All-Solid-State Battery

The  $x = 0.4$  compound with the highest lithium-ion conductivity was investigated as a solid electrolyte for an all-solid-state Li-TiS<sub>2</sub> battery. An FE-SEM image of  $0.6\text{Li}(\text{CB}_9\text{H}_{10})-0.4\text{Li}_2(\text{B}_{12}\text{H}_{12})$  ( $x = 0.4$ ) showed that the prepared compounds formed 10–20  $\mu\text{m}$  secondary particles consisting of primary particles of imperfect circular morphology with sizes ranging from  $\approx 1$  to 3  $\mu\text{m}$  (Figure S4). The primary particles were interconnected with very smooth edges. These morphologies reflect the softness and deformability of  $0.6\text{Li}(\text{CB}_9\text{H}_{10})-0.4\text{Li}_2(\text{B}_{12}\text{H}_{12})$  ( $x = 0.4$ ), which enable close contact with electrode materials during cell preparation.

Before investigating the properties of the all-solid-state batteries, we evaluated the electrochemical stability of the  $0.6\text{Li}(\text{CB}_9\text{H}_{10})-0.4\text{Li}_2(\text{B}_{12}\text{H}_{12})$  ( $x = 0.4$ ) solid electrolyte by

CV using a Mo/0.6Li(CB<sub>9</sub>H<sub>10</sub>)–0.4Li<sub>2</sub>(B<sub>12</sub>H<sub>12</sub>)/Li cell at 25 °C. The cell displayed sharp and reversible cathodic and anodic currents at approximately 0 V, which corresponded to lithium deposition ( $\text{Li}^+ + \text{e}^- \rightarrow \text{Li}$ ) and dissolution ( $\text{Li} \rightarrow \text{Li}^+ + \text{e}^-$ ), respectively (Figure 4a and Figure S5), clarifying the superior reducing ability of 0.6Li(CB<sub>9</sub>H<sub>10</sub>)–0.4Li<sub>2</sub>(B<sub>12</sub>H<sub>12</sub>) ( $x = 0.4$ ). In addition, the lack of oxidation currents within the scanned voltage range (–0.1 to 5 V) demonstrated the high electrochemical stability of 0.6Li(CB<sub>9</sub>H<sub>10</sub>)–0.4Li<sub>2</sub>(B<sub>12</sub>H<sub>12</sub>). The 0.6Li(CB<sub>9</sub>H<sub>10</sub>)–0.4Li<sub>2</sub>(B<sub>12</sub>H<sub>12</sub>) ( $x = 0.4$ ) solid electrolyte also showed stable lithium-ion transfer capability across the interface with the lithium metal anode. When galvanostatically cycled at a current density of 0.2 mA cm<sup>–2</sup> in both directions for 30 min at 25 °C, the Li/0.6Li(CB<sub>9</sub>H<sub>10</sub>)–0.4Li<sub>2</sub>(B<sub>12</sub>H<sub>12</sub>)/Li cell exhibited reversible voltage retention (9 mV) (Figure 4b,c and Figure S6). The slightly larger voltage polarization than that of the previous battery using the 0.7Li(CB<sub>9</sub>H<sub>10</sub>)–0.3Li(CB<sub>11</sub>H<sub>12</sub>) solid electrolyte [3] would be due to the lower conductivity of the 0.6Li(CB<sub>9</sub>H<sub>10</sub>)–0.4Li<sub>2</sub>(B<sub>12</sub>H<sub>12</sub>) solid electrolyte.

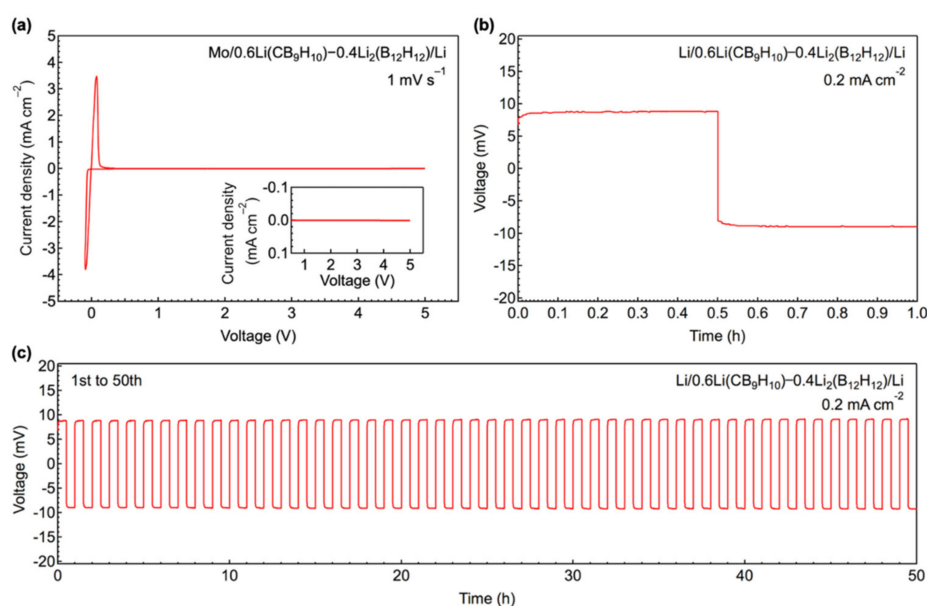


**Figure 4.** (a) Cyclic voltammetry (CV) curve of a Mo/0.6Li(CB<sub>9</sub>H<sub>10</sub>)–0.4Li<sub>2</sub>(B<sub>12</sub>H<sub>12</sub>)/Li cell at a scan rate of 1 mV s<sup>–1</sup> and scan range of –0.1 to 5.0 V (vs. Li<sup>+</sup>/Li). (Inset) Magnified profile in the high voltage region. Galvanostatic cycling profiles for (b) first and (c) prolonged cycles of a Li/0.6Li(CB<sub>9</sub>H<sub>10</sub>)–0.4Li<sub>2</sub>(B<sub>12</sub>H<sub>12</sub>)/Li cell at a current density of 0.2 mA cm<sup>–2</sup>.

For battery investigations, TiS<sub>2</sub> (theoretical capacity = 239 mAh g<sup>–1</sup>, operating voltage = 2.1 V vs Li<sup>+</sup>/Li) was used as a cathode material [31]. Figure 5a shows a schematic of the prepared all-solid-state battery. Figure 5b shows the discharge–charge profiles during the first two cycles for a rate of 0.2C (1C = 239 mA g<sup>–1</sup>). In the first cycle, the discharging and charging capacities were 236.2 and 227.3 mAh g<sup>–1</sup>, respectively. After the first cycle, highly reversible voltage profiles with a coulombic efficiency of ≈100% were retained. The second discharge capacity was 227.6 mAh g<sup>–1</sup>, which indicated 95.2% of the theoretical capacity. Compared to the battery using the 0.7Li(CB<sub>9</sub>H<sub>10</sub>)–0.3Li(CB<sub>11</sub>H<sub>12</sub>) solid electrolyte [25], the battery fabricated in this study showed the slightly lower capacity, which can be explained by the lower conductivity of the 0.6Li(CB<sub>9</sub>H<sub>10</sub>)–0.4Li<sub>2</sub>(B<sub>12</sub>H<sub>12</sub>) solid electrolyte.

The fabricated battery also presented good cycling performance. When the battery was cycled at 0.2C (47.8 mA g<sup>–1</sup>), 87.4% of the capacity (227.6 mAh g<sup>–1</sup>) in the second cycle was obtained after 20 cycles (Figure 5c and Figure S7a). In addition, for a discharging rate of 1C (239 mA g<sup>–1</sup>), the second discharging capacity was 204.2 mAh g<sup>–1</sup>, and slightly dropped to 145.5 mAh g<sup>–1</sup> after 50 cycles (Figure 5d and Figure S7b). After the first cycle, reversible voltage profiles with a coulombic efficiency of >99% were retained.

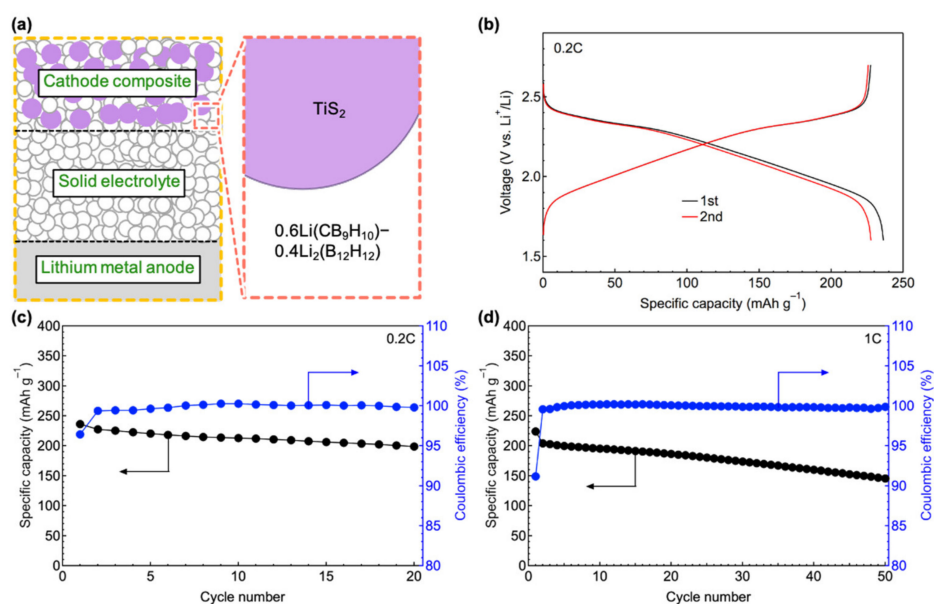


**Figure 5.** (a) Schematic of the prepared all-solid-state battery,  $\text{TiS}_2/0.6\text{Li}(\text{CB}_9\text{H}_{10})-0.4\text{Li}_2(\text{B}_{12}\text{H}_{12})/\text{Li}$ . (b) Voltage profiles for a rate of 0.2C ( $47.8 \text{ mA g}^{-1}$ ) during the first two cycles. Cycling performance in terms of discharge capacity and coulombic efficiency for rates of (c) 0.2C and (d) 1C.

#### 4. Conclusions

Similar to the  $(1-y)\text{Li}(\text{CB}_9\text{H}_{10})-y\text{Li}(\text{CB}_{11}\text{H}_{12})$  case, the high- $T$  phase stabilization in the  $(1-x)\text{Li}(\text{CB}_9\text{H}_{10})-x\text{Li}_2(\text{B}_{12}\text{H}_{12})$  quasi-binary system was observed in the low- $x$  region in which the  $[\text{CB}_9\text{H}_{10}]^-$  complex anions were partially substituted with  $[\text{B}_{12}\text{H}_{12}]^{2-}$  complex anions. In this region, increasing  $x$  promoted the high- $T$  phase formation of  $\text{Li}(\text{CB}_9\text{H}_{10})$  and thus increased the lithium-ion conductivity. Meanwhile, the  $\text{Li}(\text{CB}_9\text{H}_{10})-\text{Li}_2(\text{B}_{12}\text{H}_{12})$  solid solutions with the divalent  $[\text{B}_{12}\text{H}_{12}]^{2-}$  complex anions exhibited relatively higher activation energies and lower ionic conductivities than the  $\text{Li}(\text{CB}_9\text{H}_{10})-\text{Li}(\text{CB}_{11}\text{H}_{12})$  one with only monovalent complex anions. These composition–phase stability–conductivity dependences highlight the importance of controlling the phase transition and the ionic conductivity of the high- $T$  phase simultaneously when developing complex hydride ionic conductors. In electrochemical evaluations, the  $\text{Li}-\text{TiS}_2$  batteries fabricated using  $0.6\text{Li}(\text{CB}_9\text{H}_{10})-0.4\text{Li}_2(\text{B}_{12}\text{H}_{12})$  ( $x = 0.4$ ) solid electrolyte demonstrated good battery performance during repeated discharge–charge cycles. The insights provided in this study can potentially be applied to various complex hydride ionic conductors (e.g., Li, Na, and Mg) that exhibit a high phase-transition temperature and low ionic conductivity.

**Supplementary Materials:** The following are available online at <https://www.mdpi.com/2073-4352/11/4/330/s1>: Figure S1: Compositional dependence of the lattice volume of the  $(1-x)\text{Li}(\text{CB}_9\text{H}_{10})-x\text{Li}_2(\text{B}_{12}\text{H}_{12})$  compounds with  $0.1 \leq x \leq 0.4$ . Figure S2: Enlarged DTA curves for the  $x = 0.2$  and  $0.4$  compounds in Figure 2. Table S1: Enlarged lithium-ion conductivities at  $25^\circ\text{C}$  and activation energies of  $(1-x)\text{Li}(\text{CB}_9\text{H}_{10})-x\text{Li}_2(\text{B}_{12}\text{H}_{12})$  ( $0.1 \leq x \leq 0.5$ ). Figure S3: Arrhenius plots of the lithium-ion conductivities for the compounds with  $x = 0$  ( $\text{Li}(\text{CB}_9\text{H}_{10})$ ) and  $x = 0.4$  ( $0.6\text{Li}(\text{CB}_9\text{H}_{10})-0.4\text{Li}_2(\text{B}_{12}\text{H}_{12})$ ). Figure S4: SEM micrograph of the  $x = 0.4$  ( $0.6\text{Li}(\text{CB}_9\text{H}_{10})-0.4\text{Li}_2(\text{B}_{12}\text{H}_{12})$ ) compound. Figure S5: Cyclic voltammograms of a  $\text{Mo}/0.6\text{Li}(\text{CB}_9\text{H}_{10})-0.4\text{Li}_2(\text{B}_{12}\text{H}_{12})/\text{Li}$  cell at a scan rate of  $1 \text{ mV s}^{-1}$  during two cycles. Figure S6: Galvanostatic cycling profiles of a  $\text{Li}/0.6\text{Li}(\text{CB}_9\text{H}_{10})-0.4\text{Li}_2(\text{B}_{12}\text{H}_{12})/\text{Li}$  cell at  $0.2 \text{ mA cm}^{-2}$ . Figure S7: Discharge–charge profiles for the  $\text{TiS}_2/0.6\text{Li}(\text{CB}_9\text{H}_{10})-0.4\text{Li}_2(\text{B}_{12}\text{H}_{12})/\text{Li}$  cells for rates of (a) 0.2C and (b) 1C.

**Author Contributions:** Research design, S.K.; synthesis, S.K.; characterization, S.K. and K.K.; writing—original draft preparation, S.K.; writing—review and editing, S.K.; supervision, S.K. and S.-i.O.; funding acquisition, S.K., K.K., and S.-i.O. All authors have read and agreed to the published version of the manuscript.

**Funding:** This work was supported by JSPS KAKENHI (Grant-in-Aid for Early-Career Scientists (nos. 19K15666 and 19K15305) and Grant-in-Aid for Scientific Research on Innovative Areas “Hydrogenomics” (no. JP18H05513)) and the Collaborative Research Center on Energy Materials in IMR (E-IMR).

**Acknowledgments:** The authors would also like to thank H. Ohmiya and N. Warifune (Tohoku University) for technical assistance.

**Conflicts of Interest:** The authors declare no conflict of interest.

## References

1. Kamaya, N.; Homma, K.; Yamakawa, Y.; Hirayama, M.; Kanno, R.; Yonemura, M.; Kamiyama, T.; Kato, Y.; Hama, S.; Kawamoto, K.; et al. A lithium superionic conductor. *Nat. Mater.* **2011**, *10*, 682–686. [[CrossRef](#)] [[PubMed](#)]
2. Seino, Y.; Ota, T.; Takada, K.; Hayashi, A.; Tatsumisago, M. A sulphide lithium super ion conductor is superior to liquid ion conductors for use in rechargeable batteries. *Energy Environ. Sci.* **2014**, *7*, 627–631. [[CrossRef](#)]
3. Kim, S.; Oguchi, H.; Toyama, N.; Sato, T.; Takagi, S.; Otomo, T.; Arunkumar, D.; Kuwata, N.; Kawamura, J.; Orimo, S.-I. A complex hydride lithium superionic conductor for high-energy-density all-solid-state lithium metal batteries. *Nat. Commun.* **2019**, *10*, 1–9. [[CrossRef](#)] [[PubMed](#)]
4. Murugan, R.; Thangadurai, V.; Weppner, W. Fast Lithium Ion Conduction in Garnet-Type  $\text{Li}_7\text{La}_3\text{Zr}_2\text{O}_{12}$ . *Angew. Chem. Int. Ed.* **2007**, *46*, 7778–7781. [[CrossRef](#)]
5. Deiseroth, H.-J.; Kong, S.-T.; Eckert, H.; Vannahme, J.; Reiner, C.; Zaiss, T.; Schlosser, M.  $\text{Li}_6\text{PS}_5\text{X}$ : A Class of Crystalline Li-Rich Solids with an Unusually High  $\text{Li}^+$  Mobility. *Angew. Chem. Int. Ed.* **2008**, *47*, 755–758. [[CrossRef](#)] [[PubMed](#)]
6. Waetzig, K.; Heubner, C.; Kusnezoff, M. Reduced Sintering Temperatures of  $\text{Li}^+$  Conductive  $\text{Li}_{1.3}\text{Al}_{0.3}\text{Ti}_{1.7}(\text{PO}_4)_3$  Ceramics. *Crystals* **2020**, *10*, 408. [[CrossRef](#)]
7. Kato, Y.; Hori, S.; Saito, T.; Suzuki, K.; Hirayama, M.; Mitsui, A.; Yonemura, M.; Iba, H.; Kanno, R. High-power all-solid-state batteries using sulfide superionic conductors. *Nat. Energy* **2016**, *1*, 16030. [[CrossRef](#)]
8. Kim, S.; Hirayama, M.; Taminato, S.; Kanno, R. Epitaxial growth and lithium ion conductivity of lithium-oxide garnet for an all solid-state battery electrolyte. *Dalton Trans.* **2013**, *42*, 13112–13117. [[CrossRef](#)] [[PubMed](#)]
9. Kim, S.; Hirayama, M.; Cho, W.; Kim, K.; Kobayashi, T.; Kaneko, R.; Suzuki, K.; Kanno, R. Low temperature synthesis and ionic conductivity of the epitaxial  $\text{Li}_{0.17}\text{La}_{0.61}\text{TiO}_3$  film electrolyte. *CrystEngComm*. **2014**, *16*, 1044–1049. [[CrossRef](#)]
10. Shi, J.; Hong, Y.; Zhu, C. Effect of Chromium on Electrochemical and Mechanical Properties of  $\beta\text{-Al}_2\text{O}_3$  Solid Electrolyte Synthesized Via a Citrate-nitrate Combustion Method. *Crystals* **2020**, *10*, 987. [[CrossRef](#)]
11. Matsuo, M.; Nakamori, Y.; Orimo, S.-I.; Maekawa, H.; Takamura, H. Lithium superionic conduction in lithium borohydride accompanied by structural transition. *Appl. Phys. Lett.* **2007**, *91*, 224103. [[CrossRef](#)]
12. Kim, S.; Harada, K.; Toyama, N.; Oguchi, H.; Kisu, K.; Orimo, S.-I. Room temperature operation of all-solid-state battery using a closo-type complex hydride solid electrolyte and a  $\text{LiCoO}_2$  cathode by interfacial modification. *J. Energy Chem.* **2020**, *43*, 47–51. [[CrossRef](#)]
13. Asakura, R.; Duchêne, L.; Kühnel, R.-S.; Remhof, A.; Hagemann, H.; Battaglia, C. Electrochemical Oxidative Stability of Hydroborate-Based Solid-State Electrolytes. *ACS Appl. Energy Mater.* **2019**, *2*, 6924–6930. [[CrossRef](#)]
14. El Kharbachi, A.; Hu, Y.; Sørby, M.; Mæhlen, J.; Vullum, P.; Fjellvåg, H.; Hauback, B. Reversibility of metal-hydride anodes in all-solid-state lithium secondary battery operating at room temperature. *Solid State Ion.* **2018**, *317*, 263–267. [[CrossRef](#)]
15. Hirscher, M.; Yartys, V.A.; Baricco, M.; Von Colbe, J.B.; Blanchard, D.; Bowman, R.C.; Broom, D.P.; Buckley, C.E.; Chang, F.; Chen, P.; et al. Materials for hydrogen-based energy storage-past, recent progress and future outlook. *J. Alloy. Compd.* **2020**, *827*, 153548. [[CrossRef](#)]
16. Maekawa, H.; Matsuo, M.; Takamura, H.; Ando, M.; Noda, Y.; Karahashi, T.; Orimo, S.-I. Halide-Stabilized  $\text{LiBH}_4$ , a Room-Temperature Lithium Fast-Ion Conductor. *J. Am. Chem. Soc.* **2009**, *131*, 894–895. [[CrossRef](#)]
17. Blanchard, D.; Nale, A.; Sveinbjörnsson, D.; Eggenhuisen, T.M.; Verkuijlen, M.H.W.; Vegge, T.; Kentgens, A.P.M.; De Jongh, P.E. Nanoconfined  $\text{LiBH}_4$  as a Fast Lithium Ion Conductor. *Adv. Funct. Mater.* **2015**, *25*, 184–192. [[CrossRef](#)]
18. Oguchi, H.; Kim, S.; Maruyama, S.; Horisawa, Y.; Takagi, S.; Sato, T.; Shimizu, R.; Matsumoto, Y.; Hitosugi, T.; Orimo, S.-I. Epitaxial Film Growth of  $\text{LiBH}_4$  via Molecular Unit Evaporation. *ACS Appl. Electron. Mater.* **2019**, *1*, 1792–1796. [[CrossRef](#)]
19. Matsuo, M.; Remhof, A.; Martelli, P.; Caputo, R.; Ernst, M.; Miura, Y.; Sato, T.; Oguchi, H.; Maekawa, H.; Takamura, H.; et al. Complex Hydrides with  $(\text{BH}_4)^-$  and  $(\text{NH}_2)^-$  Anions as New Lithium Fast-Ion Conductors. *J. Am. Chem. Soc.* **2009**, *131*, 16389–16391. [[CrossRef](#)]
20. Zhang, T.; Wang, Y.; Song, T.; Miyaoka, H.; Shinzato, K.; Miyaoka, H.; Ichikawa, T.; Shi, S.; Zhang, X.; Isobe, S.; et al. Ammonia, a Switch for Controlling High Ionic Conductivity in Lithium Borohydride Ammoniates. *Joule* **2018**, *2*, 1522–1533. [[CrossRef](#)]
21. Tang, W.S.; Unemoto, A.; Zhou, W.; Stavila, V.; Matsuo, M.; Wu, H.; Orimo, S.-I.; Udovic, T.J. Unparalleled lithium and sodium superionic conduction in solid electrolytes with large monovalent cage-like anions. *Energy Environ. Sci.* **2015**, *8*, 3637–3645. [[CrossRef](#)]

22. Tang, W.S.; Matsuo, M.; Wu, H.; Stavila, V.; Zhou, W.; Talin, A.A.; Soloninin, A.V.; Skoryunov, R.V.; Babanova, O.A.; Skripov, A.V.; et al. Liquid-Like Ionic Conduction in Solid Lithium and Sodium Monocarba-closo-Decaborates Near or at Room Temperature. *Adv. Energy Mater.* **2016**, *6*, 1502237. [[CrossRef](#)]
23. Kim, S.; Toyama, N.; Oguchi, H.; Sato, T.; Takagi, S.; Ikeshoji, T.; Orimo, S.-I. Fast Lithium-Ion Conduction in Atom-Deficient closo-Type Complex Hydride Solid Electrolytes. *Chem. Mater.* **2018**, *30*, 386–391. [[CrossRef](#)]
24. Toyama, N.; Kim, S.; Oguchi, H.; Sato, T.; Takagi, S.; Tazawa, M.; Nogami, G.; Orimo, S.-I. Lithium ion conductivity of complex hydrides incorporating multiple closo-type complex anions. *J. Energy Chem.* **2019**, *38*, 84–87. [[CrossRef](#)]
25. Kim, S.; Kisu, K.; Takagi, S.; Oguchi, H.; Orimo, S.-I. Complex Hydride Solid Electrolytes of the Li(CB9H10)–Li(CB11H12) Quasi-Binary System: Relationship between the Solid Solution and Phase Transition, and the Electrochemical Properties. *ACS Appl. Energy Mater.* **2020**, *3*, 4831–4839. [[CrossRef](#)]
26. Sun, Y.; Suzuki, K.; Hori, S.; Hirayama, M.; Kanno, R. Superionic Conductors: Li<sub>10+δ</sub>[SnySi<sub>1–y</sub>]<sub>1+δ</sub>P<sub>2–δ</sub>S<sub>12</sub> with a Li<sub>10</sub>GeP<sub>2</sub>S<sub>12</sub>-type Structure in the Li<sub>3</sub>PS<sub>4</sub>–Li<sub>4</sub>SnS<sub>4</sub>–Li<sub>4</sub>SiS<sub>4</sub> Quasi-ternary System. *Chem. Mater.* **2017**, *29*, 5858–5864. [[CrossRef](#)]
27. Tang, W.S.; Yoshida, K.; Soloninin, A.V.; Skoryunov, R.V.; Babanova, O.A.; Skripov, A.V.; Dimitrievska, M.; Stavila, V.; Orimo, S.-I.; Udovic, T.J. Stabilizing Superionic-Conducting Structures via Mixed-Anion Solid Solutions of Monocarba-closo-borate Salts. *ACS Energy Lett.* **2016**, *1*, 659–664. [[CrossRef](#)]
28. Orimo, S.-I.; Nakamori, Y.; Eliseo, J.R.; Züttel, A.A.; Jensen, C.M. Complex Hydrides for Hydrogen Storage. *Chem. Rev.* **2007**, *107*, 4111–4132. [[CrossRef](#)]
29. Zhu, Y.; He, X.; Mo, Y. Origin of Outstanding Stability in the Lithium Solid Electrolyte Materials: Insights from Thermodynamic Analyses Based on First-Principles Calculations. *ACS Appl. Mater. Interfaces* **2015**, *7*, 23685–23693. [[CrossRef](#)]
30. Yoo, H.D.; Shterenberg, I.; Gofer, Y.; Gershinshy, G.; Pour, N.; Aurbach, D. Mg rechargeable batteries: An on-going challenge. *Energy Environ. Sci.* **2013**, *6*, 2265–2279. [[CrossRef](#)]
31. Whittingham, M.S. Electrical Energy Storage and Intercalation Chemistry. *Science* **1976**, *192*, 1126–1127. [[CrossRef](#)] [[PubMed](#)]